JCI insight

Myofibroblast de-differentiation proceeds via distinct transcriptomic and phenotypic transitions

Sean M. Fortier, … , Giovanni Ligresti, Marc Peters-Golden

JCI Insight. 2021. https://doi.org/10.1172/jci.insight.144799.

Research In-Press Preview **Cell biology** **Pulmonology**

Graphical abstract

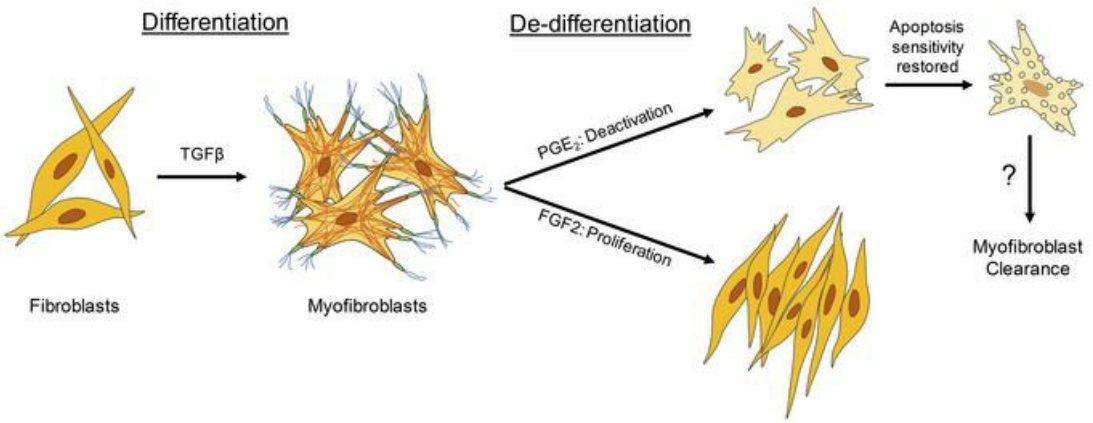

Myofibroblast de-differentiation proceeds via distinct transcriptomic and phenotypic transitions

Sean M. Fortier[1], Loka R. Penke[1], Dana King[2], Tho X. Pham[3], Giovanni Ligresti[3], Marc Peters-Golden[1*]

[1]Division of Pulmonary and Critical Care Medicine, and [2]BCRF Bioinformatics Core, University of Michigan, Ann Arbor, Michigan. [3]Department of Medicine, Boston University School of Medicine, Boston, MA.

*Corresponding Author

Marc Peters-Golden, M.D.

6301 MSRB III

1150 W. Medical Center Drive

Ann Arbor, MI 48109-5642, USA

Email: petersm@umich.edu

Phone: 734-936-5047

Fax: 734-764-4556

The authors have declared that no conflict of interest exists.

Abstract

Myofibroblasts are the major cellular source of collagen, and their accumulation – via differentiation from fibroblasts and resistance to apoptosis – is a hallmark of tissue fibrosis. Clearance of myofibroblasts by de-differentiation and restoration of apoptosis sensitivity has the potential to reverse fibrosis. Prostaglandin E_2 (PGE_2) and mitogens such as FGF2 have each been shown to de-differentiate myofibroblasts, but the resultant cellular phenotypes have neither been comprehensively characterized nor compared. Here we show that PGE_2 elicited de-differentiation of human lung myofibroblasts via cAMP/PKA while FGF2 utilized MEK/ERK. The two mediators yielded transitional cells with distinct transcriptomes, with FGF2 promoting but PGE_2 inhibiting proliferation and survival. The gene expression pattern in fibroblasts isolated from the lungs of mice undergoing resolution of experimental fibrosis resembled that of myofibroblasts treated with PGE_2 in vitro. We conclude that myofibroblast de-differentiation can proceed via distinct programs exemplified by treatment with PGE_2 and FGF2, with that occurring in vivo most closely resembling the former.

Introduction

Fibrosis is the consequence of a disordered and pathologic host response to tissue injury that affects all organ systems and is associated with a high morbidity and mortality (1, 2). Idiopathic pulmonary fibrosis (IPF) is a severe and progressive lung disease characterized by parenchymal scarring that leads to architectural distortion, respiratory failure, and death (3). The ultimate effector cell of fibrotic disorders is the myofibroblast – a large stellate-shaped cell with numerous exocytotic vesicles, focal adhesions, and stress fibers composed of alpha-smooth muscle actin (αSMA). Lung myofibroblasts originate predominantly from resident fibroblasts whose further phenotypic differentiation is driven by pro-fibrotic mediators, such as TGFβ. These cells promote fibrosis and tissue stiffness by virtue of their capacity to secrete abundant quantities of various extracellular matrix proteins such as collagens, elastin, and fibronectin and via their contractile function (4, 5). An additional important characteristic feature of myofibroblasts in IPF and other fibrotic disorders is their resistance to apoptosis, which contributes to their accumulation in involved tissues (6, 7). This accumulation of myofibroblasts contrasts with their eventual clearance during normal wound healing, thus allowing fibrosis to persist and progress (8).

Patients diagnosed with IPF usually come to clinical attention only after fibrosis is already established. Unfortunately, current therapies fail to reverse established fibrosis, in part because they do not eliminate the activated myofibroblasts that have accumulated. Although myofibroblasts were historically considered to be terminally differentiated cells, their capacity for de-differentiation, defined as the loss of αSMA stress fibers, is now well-recognized and has been implicated as being necessary for fibrosis resolution (9).

The two substances best-established to promote de-differentiation are the soluble mediators prostaglandin E_2 (PGE_2) (10-12) and mitogens such as FGF2 (13, 14). However, it is currently unclear how these two categories of molecules – which signal in entirely different ways – orchestrate the phenotypic transition of myofibroblasts. In the present study, we investigated this by performing mechanistic, RNA-seq, and functional studies on PGE_2- and FGF2-treated human lung myofibroblasts examined in parallel. While treatment with PGE_2 and FGF2 both downregulated hallmark fibrotic genes such as αSMA, collagen I, and fibronectin, they did so by generating distinct transitional cellular phenotypes, characterized by unique gene programs with differing capacities for proliferation and apoptosis. Finally, the gene signatures defined by RNA-seq of fibroblasts isolated from the lungs of young mice with resolving bleomycin-induced fibrosis

were compared to those of myofibroblasts de-differentiated in vitro, and found to more closely resemble those observed in cells treated with PGE_2 than with FGF2.

Results

PGE_2 utilizes the EP2/cAMP/PKA pathway to de-differentiate myofibroblasts whereas FGF2 requires MEK/ERK

The abilities of PGE_2 and FGF2 to elicit myofibroblast de-differentiation have been studied individually but have not previously been directly compared. As depicted in the experimental scheme in Figure 1A, myofibroblasts were first established by treating normal adult human lung fibroblasts with TGFβ for 48 h in serum-free medium, followed by subsequent addition of PGE_2 or FGF2 to initiate de-differentiation. We initially evaluated the effects of each treatment on the characteristic fibrosis-associated protein and myofibroblast marker αSMA. As expected, myofibroblasts expressed much higher levels of αSMA protein than did fibroblasts. Moreover, both PGE_2 and FGF2 reduced the expression of αSMA protein at 5 d. Notably, PGE_2 elicited a greater decline in αSMA (Figure 1B). In parallel with this global decline in αSMA protein, its assembly into stress fibers – an essential component of the myofibroblast contractile machinery – was also disrupted by treatment with PGE_2 and FGF2 (Figure 1C). These results confirm that PGE_2 and FGF2 each have the capacity to de-differentiate myofibroblasts.

We confirmed that they elicited parallel reductions in αSMA mRNA (*ACTA2*), as well as the highly expressed myofibroblast genes collagen I (*COL1A1*) and fibronectin (*FN1*), when analyzed at 24 h and 48 h, respectively (Figure 1, D and E). These time points were selected based on observed differences in the de-differentiation kinetics triggered by the two mediators in pilot experiments. It is notable that this shared outcome for both mediators occurs despite marked differences in their molecular identity, the characteristics of their cognate receptors, and second messenger signaling cascades. PGE_2 is a prostaglandin lipid mediator known to interact with four E-prostanoid GPCRs (EP 1-4) which signal through the second messengers cAMP or calcium (15). In contrast, FGF2 signals through a receptor tyrosine kinase affecting multiple downstream pathways including PI3K, protein kinase B (AKT), and the MAPKs (16). We therefore investigated the signaling pathways involved in PGE_2- and FGF2-mediated myofibroblast de-differentiation. We have shown previously that PGE_2 prevents TGFβ-induced fibroblast differentiation mainly by activation of the EP2 receptor, which stimulates adenylate cyclase to increase production of intracellular cAMP and activate protein kinase A (PKA) (17-19). Accordingly, we examined the abilities of these same signaling pathway components of PGE_2 to elicit myofibroblast de-differentiation. Both butaprost, a PGE_2 analog that specifically

activates EP2, and forskolin, a direct activator of adenylate cyclase, reduced levels of *ACTA2*, *COL1A1*, and *FN1* (Figure 1, D and E). cAMP can act via two effector proteins, PKA and the guanine nucleotide exchange protein activated by cAMP (Epac). A cAMP analog that selectively activates PKA (6-BNZ cAMP) was also capable of de-differentiation, whereas one that selectively activates Epac (8-pCPT cAMP) was not. Next we explored FGF2 signaling and found that its ability to reduce expression of αSMA and collagen was overcome by inhibition of the MEK/ERK pathway (Figure 1E, Supplemental Figure 1A), but not by inhibition of the MAPKs p38 or JNK, or by inhibition of AKT (Supplemental Figure 1B). The distinctiveness of the signaling pathways by which the two mediators exert their effects is underscored by the fact that the effects of PGE_2 were not abolished by treatment with the ERK inhibitor U0126 (Supplemental Figure 1C). The modest reduction in *FN1* by FGF2 was not abolished by inhibition of MEK/ERK, p38, JNK, or AKT (Supplemental Figure 1D). The signaling mechanisms by which PGE_2 and FGF2 promote myofibroblast de-differentiation are summarized in Figure 1F.

Transcriptome profiling of PGE_2- and FGF2-treated myofibroblasts via RNA-seq

Although we previously utilized microarray analysis to describe the transcriptomic effects of PGE_2 in TGFβ-elicited myofibroblasts (12), that analysis lacked a comprehensive examination of non-coding RNAs as well as a comparison with the effects of FGF2. The fact that PGE_2 and FGF2 led to myofibroblast de-differentiation by exploiting different signaling pathways provided the impetus to undertake a more comprehensive examination that might reveal differences in the transitional cell phenotypes that they elicit. We interrogated this possibility using RNA-seq to characterize genome-wide transcriptomic changes in myofibroblasts treated with either PGE_2 or FGF2. We sought to characterize early and comparable phases of the phenotypic transition promoted by PGE_2 and FGF2. The time point arbitrarily chosen for analysis was that which yielded a ~50% reduction in *ACTA2*, determined to be 6 h for PGE_2 and 24 h for FGF2 (Figures 2A and 6B). Each treatment condition was paired with a time-matched untreated myofibroblast control, and all analyses were performed in triplicate cultures. A total of 17,903 distinct RNA transcripts (excluding small RNAs) were detected. A high degree of concordance was observed among the triplicate samples from each treatment condition (Supplemental Figure 2). PGE_2 differentially regulated 3105 genes and FGF2 differentially regulated 1720 genes, as compared to their corresponding time-matched untreated controls. Of these, PGE_2 upregulated

1521 genes and downregulated 1584 whereas FGF2 upregulated 878 and downregulated 842 (Figure 2B). PGE_2 exhibited higher log-fold changes among top regulated mRNAs than did FGF2, with only one gene, *DEPP1*, a regulator of autophagy (20), shared among the top 25 genes up- or downregulated by both mediators (Supplemental Table 1)**.** Despite their distinct actions, PGE_2 and FGF2 mutually regulated 716 genes in common (Figure 2C). Principle components analysis showed similar clustering between 6 and 24 h untreated controls, but marked differences between myofibroblasts treated with PGE_2 vs. FGF2, as well as between each agent and the untreated controls (Figure 2D).

Effects of PGE_2 and FGF2 on myofibroblast signaling pathways and gene ontology

We employed KEGG pathway enrichment analysis to characterize and compare the gene expression patterns of the transitional cellular phenotypes evoked by treatment of myofibroblasts with PGE_2 and FGF2. Of the KEGG pathways included in our analysis, PGE_2 and FGF2 each enriched 46 pathways, 17 of which were shared (Supplemental Table 2). From these, we curated a list of pathways lacking disease specificity, extra-pulmonary organ selectivity, and functional redundancy

(Table 1). Of these 22 remaining pathways, 15 were enriched by PGE_2, 16 were enriched by FGF2, and 8 pathways were enriched by both.

Among the pathways uniquely enriched by PGE_2 were MAPK and mTOR. Each has been shown to be involved in fibroblast biology in the context of pulmonary fibrosis (21, 22) with mTOR representing a potential target for anti-fibrotic therapy (23). In contrast, FGF2 predictably enriched cell cycle, apoptosis, and adhesion/anchoring pathways. Of particular interest were cellular functions enriched by both PGE_2 and FGF2, given the possibility that a common pathway downstream of cAMP/PKA and MEK/ERK may participate in mediating the de-differentiating effects of each molecule. Indeed, both PGE_2 and FGF2 significantly impacted the fibrosis-associated pathways TGFβ, WNT, and PI3K-AKT. Notably, cAMP signaling was enriched by FGF2 as well as PGE_2 (Table 1).

As TGFβ plays an integral role in the initiation, maintenance, and progression of pulmonary fibrosis (24-26), we specifically examined and compared the regulation of known TGFβ-associated genes. Broadly, PGE_2 downregulated 21 TGFβ pathway genes while FGF2 downregulated 10 (Figure 3). The canonical TGFβ effectors *SMAD3*, *SMAD7*, and *SMAD9* were downregulated by PGE_2 while FGF2 downregulated *SMAD7* and *SMAD9* without significant regulation of *SMAD3*.

Notably, the NADPH oxidase gene *NOX4* – a central mediator of myofibroblast differentiation, ECM protein production, and contractility (27) – was downregulated by both effector molecules.

We next compared differentially expressed genes belonging to the remaining mutually enriched pathways (Figure 3). PGE_2 and FGF2 upregulated cytokines such as *IL6*, *IL11*, and *CCL2* while downregulating *IL16* and *IL6R*. Interestingly, *SOCS3* – which opposes IL6 signaling by inhibiting JAK-STAT – was upregulated by PGE_2 and downregulated by FGF2. Though many genes belonging to the cAMP signaling pathway were regulated in parallel by each treatment, the hallmark PKA-induced early gene *FOS* was repressed by FGF2 while *JUN*, whose protein product commonly binds FOS to form the AP-1 complex, was repressed by PGE_2. It is notable that both of these subunits of the archetypal AP-1 heterodimer – which has been shown to promote fibrosis (28, 29) – were reduced by either PGE_2 or FGF2. The WNT-associated genes *NFATC2*, *FZD1*, *FZD9* and *WISP1* were upregulated by both treatments whereas *WNT5A*, *WNT5B*, *WNT10B*, and *WNT11* were induced by PGE_2 and repressed by FGF2. The growth factors *FGF1*, *FGF5*, and *PDGFB* were all downregulated by PGE_2 and upregulated by FGF2 whereas *HGF*, shown to be anti-fibrotic (30) and deficient in IPF fibroblasts (31), was upregulated by PGE_2 but downregulated by FGF2. These results highlight many

differences in gene regulation between PGE_2 and FGF2, even within mutually enriched pathways.

As discussed above, tissue contraction, ECM protein secretion, and apoptosis resistance are cardinal features of myofibroblasts. We therefore specifically interrogated the gene ontologies associated with these biologic processes. First, we found that PGE_2, and to a lesser extent FGF2, downregulated a number of important cytoskeletal, focal adhesion, and ECM related genes (Figure 4A) including *ACTA2* and *ACTN1*. Both treatments reduced the expression of *MRTF1*, a transcription factor crucial for TGFβ-induced expression of αSMA in lung myofibroblasts (17). Neither treatment resulted in a significant change in *FN1* or *COL1A1* expression at the early time points at which sequencing analysis was performed, although each of these transcripts was reduced at later time-points (Figure 1). Notably, PGE_2 suppressed the focal adhesion mediators *VASP*, *VLC*, *TLN1*, and *CTHRC1* while FGF2 increased the expression of each. Though focal adhesion kinase (*PTK2*) was not significantly modulated by either treatment, the related gene *PTK2B*, which has similar biologic endpoints as *PTK2* (32), was markedly downregulated by both. Modulation of the extracellular matrix metalloproteases (MMPs) and their inhibitors (TIMPs) was heterogeneous between treatments other than the mutual suppression of *MMP25* and *MMP28*.

Finally, the pleiotropic growth factor *CTGF* was inversely regulated – decreased by PGE_2 and induced by FGF2.

Cellular differentiation and proliferation have long been considered to represent opposing or even mutually exclusive cellular programs (33). Indeed, it has been suggested that such a mechanism is integral to the ability of mitogens such as FGF2 to promote de-differentiation (9). Predictably, myofibroblasts treated with FGF2 upregulated multiple cell cycle genes including cyclins (*CCNB1*, CCNB*2*, *CCND1, CCND2*, and *CCNE2*), cyclin dependent kinases (*CDK1, CDK2, CDK7*), and *FOXM1* – a critical transcription factor in fibroblast proliferation (34) (Figure 4B). By contrast, PGE_2, which is well-known to inhibit mesenchymal cell proliferation (33, 35, 36), exerted minimal effects on the expression of these genes and upregulated the cyclin dependent kinase inhibitors *CDKN1C* and *CDKN2C*. Consistent with its pro-proliferative effects, FGF2 increased pro-survival genes such as *BIRC5* and *MYC* whereas PGE_2 increased the pro-apoptotic genes *APAF1* and *CASP9*. Finally, the pro-fibrotic protein *SERPINE1*, well-known to be overexpressed in IPF fibroblasts and reported to contribute to apoptosis resistance in myofibroblasts (37), was downregulated by PGE_2 but upregulated by FGF2 (Figure 4B). These results indicate that PGE_2 and FGF2 have largely opposing effects on genes involved in proliferation and apoptosis.

PGE_2 and FGF2 modulate the expression of fibrosis-associated long non-coding RNAs and microRNAs in myofibroblasts

Non-coding RNAs (ncRNAs) play a significant role in post-transcriptional regulation as well as the determination and maintenance of cell phenotypes (38). Among these, a number of miRNAs exert pro- or anti-fibrotic effects by inhibiting translation and promoting RNA degradation (39, 40). Similarly, many long non-coding RNAs (lncRNAs) influence fibrosis through various mechanisms including miRNA "sponging" – preventing miRNA-mRNA interactions by competitive binding (41). Of the more than 8800 total lncRNAs identified, PGE_2 and FGF2 modulated 811 and 261, respectively, with 100 shared among them (Figure 5A and 5B). The top 25 regulated lncRNAs are listed in Supplemental Table 3. We curated a list of fibrosis-associated lncRNAs regulated by at least one of our treatments (Figure 5C). Both treatments downregulated *NEAT1* and *DNM3OS*, while PGE_2 reduced the pro-fibrotic *PCAT1* and *PVT1*, and FGF2 reduced *MALAT1*. The abundant lncRNAs *NEAT1* and *MALAT1* have been shown to contribute to organ fibrosis and to sponge numerous miRNAs (42, 43) while *DNM3OS* has been reported to promote the expression of the pro-fibrotic miRNAs 214-3p and 199a-3p/5p in

human lung fibroblasts (44). PGE_2 also increased the anti-fibrotic lncRNA *FENDRR*, which sponges miR-214-3p, and is known to be reduced in IPF fibroblasts (45).

Though over 350 miRNAs were detected under each treatment condition, PGE_2 only significantly modulated 3 miRNAs while FGF2 regulated 23 (Figure, D and E, Supplemental Table 4). Both PGE_2 and FGF2 increased expression of miR-543 which has been shown to inhibit TGFβ activation and gene expression in rat cardiac fibroblasts (46). miR-335-3p, an anti-proliferative and pro-apoptotic miRNA with anti-fibrotic properties in gingival fibroblasts (47, 48), was upregulated by PGE_2 and repressed by FGF2. The top PGE_2-upregulated miRNA, miR-129-5p, exhibits anti-fibrotic actions in dermal fibroblasts by targeting *COL1A1* (49). Furthermore, FGF2 upregulated the anti-fibrotic miR-29b-3p/5p, miR-152-5p, and let-7a-3p (5, 50, 51) while downregulating the pro-fibrotic miR-145-3p (52). Other pro- and anti-fibrotic-associated miRNAs – including miR-21 (53), miR-27a-3p/miR-27b-3p (54), were detected in high abundance in our analysis but were not differentially regulated by either treatment (Supplemental Table 5). As discussed above, miRNA activity can be regulated through RNA sponging without changes in miRNA expression (38, 55). Indeed, multiple differentially expressed lncRNAs in our analysis have been shown to affect the function of a number of fibrosis-associated miRNAs that were not themselves

differentially regulated in our study (Table 2). These data indicate a possible role for ncRNAs in PGE_2 and FGF2 mediated de-differentiation of myofibroblasts.

Myofibroblasts treated with PGE_2 and FGF2 separately or in combination produce distinct cellular morphologies and fibrosis-associated gene expression patterns

To complement their distinct transcriptomic effects, we sought to examine the influence of PGE_2 and FGF2 on myofibroblast morphology. Furthermore, we wished to determine the net effect of combining these two effector molecules – a closer approximation of the in vivo conditions in which they would be expected to coexist – on cell morphology, loss of stress fibers, and the expression of various fibrosis-associated genes. Undifferentiated fibroblasts stained with the membrane dye PKH26 appeared spindle-shaped and elongated in stark contrast to the larger, cuboidal, and stellate-shaped, myofibroblasts (Figure 6A). Compared to untreated myofibroblasts, those subsequently exposed to PGE_2 appeared smaller, thinner, and displayed fewer cytoplasmic projections. FGF2-treated myofibroblasts lost their stellate shape, appearing thin and elongated similar to native fibroblasts. The combination of PGE_2 and FGF2 produced a small,

more rounded cell, distinct from the transitional cell morphology produced by either treatment alone. We assessed the kinetics of *ACTA2* in response to each treatment as well as their combination (Figure 6B). Combined treatment displayed an effect that was statistically greater than that with either alone at 24, 48, and 72 h. Interestingly, though PGE_2 treatment resulted in a more rapid reduction in *ACTA2* through 24 h, its effects plateaued at 48 h whereas FGF2 progressively reduced *ACTA2* through 72 h. Combined treatment also reduced αSMA protein and its organization into stress fibers (Figure 6C) to an extent apparently greater than did either treatment alone (Figure 1B). We next performed qPCR on selected fibrotic genes to further evaluate the effect of combined treatment on each (Figure 6D). As displayed in Figure 6B, combined treatment with PGE_2 and FGF2 reduced *ACTA2* at 24 h to a greater extent than either treatment alone. There was a trend toward an additive reduction in *COL1A1*. *FN1* reduction in response to PGE_2 and FGF2 appeared comparable in magnitude to PGE_2 alone. Though the pro-fibrotic growth factor *CTGF* and focal adhesion regulator *VASP* were each downregulated by PGE_2 and upregulated by FGF2, combination treatment resulted in reduced expression of each transcript. Expression of *NOX4* was reduced in PGE_2- and FGF2-treated myofibroblasts, though combination treatment did not yield any further reduction.

PGE_2 and FGF2 have opposite effects on myofibroblast proliferation and apoptosis

Our transcriptomic analysis predicted that treatment of myofibroblasts with PGE_2 would inhibit their capacity for proliferation and re-establish apoptosis sensitivity, while treatment with FGF2 would promote proliferation and maintain apoptosis resistance. We tested these predictions by directly assaying proliferation capacity and apoptosis sensitivity in myofibroblasts treated with PGE_2 and/or FGF2 as compared to untreated controls. First, we assessed the expression of cell cycle genes (Figure 7A, top panel) and apoptosis genes (Figure 7A, bottom panel) in myofibroblasts exposed to each treatment alone and in combination. *CCNB2*, *CCND1,* and *FOXM1* were upregulated by FGF2, consistent with our RNA-seq data. Importantly, though PGE_2 did not significantly modulate these genes, it negated their upregulation by FGF2. Conversely, the expression of the cyclin dependent kinase inhibitor *CKDN1C* was greatly and uniquely increased by PGE_2, an increase not fully abrogated by addition of FGF2. The anti-apoptotic genes *BIRC5* and *SERPINE1* were each uniquely upregulated by FGF2, but such increases were partially or completely abrogated by the addition of PGE_2, while *MYC* was

downregulated by PGE_2 in the presence or absence of FGF2. The pro-apoptotic gene *CASP9*, which leads to activation of CASP3 (56), was upregulated by PGE_2, downregulated by FGF2, and remained slightly upregulated with combined treatment. Taken together, these data demonstrate that PGE_2 and FGF2 have opposing effects on myofibroblast genes associated with proliferation and apoptosis.

We next determined if these transcriptomic differences were associated with functional differences in myofibroblast proliferation and apoptosis. Consistent with the effect of each treatment on cell cycle genes, FGF2 increased the proliferation of established myofibroblasts, whereas PGE_2 had no effect relative to untreated myofibroblasts but abolished the proliferative effects of FGF2 (Figure 7B). To assess the apoptosis sensitivity of myofibroblasts undergoing de-differentiation, we treated cells with PGE_2 and/or FGF2 for 5 d prior to treatment with the anti-Fas activating antibody; apoptosis was assessed by Western blot detection of cleaved/total CASP3 and PARP within cell lysates (Figure 7C). As expected, the levels of cleaved CASP3 and PARP did not increase in response to Fas activation of untreated myofibroblasts, highlighting their intrinsic resistance to apoptosis. In contrast, myofibroblasts de-differentiated with PGE_2 displayed significantly higher levels of cleaved CASP3 and PARP after exposure to anti-Fas

activating antibody relative to untreated myofibroblasts. Such an effect was not seen in myofibroblasts de-differentiated with FGF2, but was preserved in myofibroblasts de-differentiated with both agents together. To assess whether restoration of apoptosis sensitivity in myofibroblasts elicited by PGE_2 depends on prior de-differentiation, we performed immunofluorescence microscopy for annexin V and αSMA in PGE_2-treated myofibroblasts and untreated myofibroblast controls subsequently exposed to anti-Fas for 4 h (Supplemental Figure 3). Notably, we found a small proportion of PGE_2-treated myofibroblasts that retained their stress fibers, suggesting underlying fibroblast heterogeneity. PGE_2-treated myofibroblasts undergoing apoptosis – defined by annexin V staining – were almost exclusively limited to those lacking αSMA stress fibers. Untreated myofibroblasts did not exhibit annexin V staining, further confirming their resistance to apoptosis.

Lung fibroblasts from an in vivo model of fibrosis resolution exhibit similar gene signatures as those determined in myofibroblasts de-differentiated in vitro

The RNA-seq data presented thus far was derived from in vitro treatment of myofibroblasts with individual mediators. To evaluate the relevance of these

findings in a less reductionist and in vivo model of fibrosis resolution, we compared the transcriptome of freshly isolated lung fibroblasts from young mice with that of lung fibroblasts isolated from aged mice following bleomycin challenge. It has been established that, in contrast to aged mice, young mice subjected to bleomycin-induced pulmonary fibrosis can undergo spontaneous resolution – in which fibroblasts reduce collagen secretion and lose their αSMA stress fibers (57-59). To characterize their global transcriptome, RNA-seq was performed on FACS-sorted fibroblasts isolated from the lungs of young mice (2 mo) and aged mice (18 mo) during the early phase of fibrosis resolution (30 d post-bleomycin) (Figure 8A). A comprehensive analysis of this data is described in a separate manuscript currently in preparation; herein we present limited data from this dataset relevant to cell cycle, apoptosis, and focal adhesion genes found to be significantly modulated by either PGE_2 or FGF2 treatment of myofibroblasts in vitro (Figure 4A and 4B). Gene expression changes in fibroblasts isolated from young lungs undergoing fibrosis resolution were expressed relative to those of fibroblasts isolated from aged mouse lungs with non-resolving fibrosis (Figure 8B).

Lung fibroblasts sorted from mouse lungs undergoing fibrosis resolution expressed lower levels of proliferation genes including *Ccnb1*, *Ccnb2*, *Ccnd1*, *Ccne1*, *Cdk1*, and *Foxm1*. Conversely, the anti-proliferative *Cdkn1c* was

upregulated. Five of the eighteen significantly modulated cell cycle genes in fibroblasts from mice with resolving fibrosis were regulated in parallel to PGE_2-treated human myofibroblasts, while just one gene was regulated in parallel to FGF2-treated myofibroblasts. Notably, fifteen of these eighteen cell cycle genes were regulated oppositely to that of FGF2-treated myofibroblasts in vitro whereas only three genes were regulated opposite to PGE_2-treated myofibroblasts. The pro-apoptotic gene *Casp9* was upregulated in fibroblasts from mice with resolving fibrosis and the pro-survival genes *Birc5*, *Birc3*, and *Serpine1* were all downregulated. Of the ten apoptosis-associated genes significantly modulated in young lung fibroblasts, three were regulated in parallel with PGE_2-treated versus one in FGF2-treated myofibroblasts. Interestingly, the apoptosis-associated genes *Myc*, *Bcl2l1*, *Bcl2l11*, and *Tnfrsf8* – which were regulated oppositely by PGE_2 and FGF2 in vitro – showed no significant differences between fibroblasts isolated from mice with resolving and non-resolving fibrosis, suggesting an in vivo level of expression reflecting the arithmetic sum of changes elicited individually by PGE_2 and FGF2 in vitro. Eight of ten significantly modulated focal adhesion genes were also downregulated in parallel with the PGE_2-treated myofibroblasts. Among these were *Vasp* – a phosphoprotein involved in actin assembly and SRF activity (60) – and *Cthrc1* – a marker of tissue fibrosis (61). In contrast, FGF2-treated

myofibroblasts showed opposite regulation of *Vasp, Vcl, Tln,* and *Cthrc1*. *Col1a1* and *PTK2B* were the only genes assessed among these pathways that were concordantly regulated by PGE_2 and FGF2 treatment of myofibroblasts in vitro as well as in fibroblasts from mice during fibrosis resolution.

Discussion

Myofibroblasts are critical effector cells that orchestrate, maintain, and propagate lung scarring in IPF and other fibrotic disorders (62). Whereas inhibiting the fibroblast to myofibroblast transition has the potential to prevent fibrogenesis in response to a recognized injury and to arrest progression of an established fibrotic process, it is unlikely to be sufficient to promote its resolution. By contrast, promoting myofibroblast clearance has the potential to do so. As elimination of myofibroblasts in fibrotic diseases is limited by their resistance to apoptosis, de-differentiation provides a potential route to restore apoptosis sensitivity and thus facilitate myofibroblast removal. Indeed, myofibroblast de-differentiation has been reported in response to a variety of effector molecules, including mitogens such as serum and FGFs (13, 14), lipid mediators PGE_2 and PGI_2 (10, 63), statins (64), siRNA knockdown of the transcription factors MyoD (33) and FOXM1 (34), and the bromodomain inhibitor JQ1 (65). Whether de-differentiation with these diverse classes of effector molecules yields common or divergent transitional cell phenotypes has not previously been explored. Here, we compared the operative signaling mechanisms, as well as the transcriptomic, morphologic, and functional characteristics, of myofibroblasts treated with the endogenous soluble mediators PGE_2 and FGF2.

Our results confirm that PGE_2 and FGF2 are both capable of de-differentiating human lung myofibroblasts by downregulating αSMA and eradicating stress fibers (Figure 1, B and C). However, they accomplish this via distinct signaling pathways and with different kinetics (Figure 1, B, D, and E, and Figure 6B). Globally, PGE_2 modulated nearly double the number of protein-coding genes, nearly triple the number of non-coding RNAs, and induced greater log-fold changes among top regulated genes than did FGF2 (Figure 2B, Figure 5A, and Supplemental Table 1). Moreover, each mediator produced a unique transitional cell phenotype characterized by distinctive gene programs, morphology, proliferative capacities, and sensitivity to apoptosis (Figures 3-7).

It is now recognized that myofibroblasts have multiple potential fates (8, 66-68). While myofibroblast senescence favors their persistence and thus progression of fibrotic disease (9), we demonstrate herein that deactivation and proliferation represent two distinct paths by which myofibroblasts can de-differentiate. As in prior studies establishing that PGE_2 inhibits many critical functions of *fibroblasts* – including proliferation, differentiation, contractility, and focal adhesion (17, 19, 69) – we show here that PGE_2 also deactivates these same processes in *myofibroblasts* (Figures 1, 3, 4, and 7). By contrast, the potent fibroblast mitogen FGF2 (34) stimulates proliferation in myofibroblasts (Figure 4B, and Figure 7, A

and B). These comparative data suggest that while FGF2 de-differentiates lung myofibroblasts primarily by promoting their proliferation, PGE_2 accomplishes this via a much more global form of cellular deactivation. A major and functionally important consequence of these divergent mechanisms of de-differentiation is that transitional cells resulting from PGE_2 exposure are more, while those resulting from FGF2 exposure are less, susceptible to apoptosis (Figure 7C).

It is likely that in order to undergo cell division, de-differentiating myofibroblasts must restructure their cytoskeletal network and matrix interactions. Indeed, FGF2 downregulated αSMA, stress fibers, and collagen in established myofibroblasts via activation of the MEK/ERK pathway (Figure , D and E), which has also been previously shown to mediate proliferation in myofibroblasts (33). Morphologically, FGF2-treated myofibroblasts elongate and lose their stellate shape, resembling native fibroblasts (Figure 6A). Overexpression of FGF2 has similarly been reported to inhibit myofibroblast differentiation in vitro and pulmonary fibrosis in vivo (14). In contrast to the mechanisms of action of FGF2, PGE_2 de-differentiates myofibroblasts (Figure 1D) while concomitantly inhibiting their proliferation (Figure 7B), effects likely to be mediated through cAMP/Epac (35), rather than ERK (Supplemental Figure 1C). In addition to our current findings and our previously published microarray data (12) demonstrating that

PGE_2 remodels the global transcriptome of established myofibroblasts, the importance of cAMP signaling in this regard is further validated by recent parallel findings with a PGI_2 analog acting via its G_s-coupled receptor (63).

In addition to modulating mRNA expression, PGE_2 and FGF2 differentially regulated multiple lncRNAs and miRNAs in lung myofibroblasts (Figure 5). Several ncRNAs modulated in our study have been reported to influence myofibroblast function and fibrotic outcomes. Importantly, many anti-fibrotic miRNAs that were not significantly modulated by either treatment do in fact interact with lncRNAs modulated by PGE_2 and/or FGF2 (Table 2). The ncRNAs encompass a large family of pleiotropic post-transcriptional regulators that control the expression of gene programs through complex lncRNA-miRNA-mRNA interactions (70, 71). We therefore speculate that lncRNAs and miRNAs may be important for the effects of both PGE_2 and FGF2 in myofibroblasts. Their coordinated actions remain to be more comprehensively defined and these data provide a blueprint for doing so in future studies.

Since myofibroblast de-differentiation elicited by PGE_2 and FGF2 – expected constituents of an injured/fibrotic lung (72, 73) – proceeded via distinct signaling mechanisms and gene expression programs, we assessed their individual and

combined effects on *ACTA2* kinetics, myofibroblast morphology, de-differentiation, proliferation, and apoptosis sensitivity. Indeed, myofibroblasts treated with both mediators displayed an additive reduction in αSMA mRNA, protein, and stress fibers (Figure 6, B and C), while also exhibiting a morphology distinct from that of either treatment alone (Figure 6A). The effects of combined versus individual treatment on specific fibrosis-associated genes ranged from additive inhibition (*ACTA2*) to no additive effect (*NOX4*) to a dominant effect of PGE_2 (*CTGF* and *VASP*) (Figure 6D). Moreover, PGE_2 functioned to negate the proliferative and anti-apoptotic effects of FGF2 (Figure 7).

The inherently reductionist nature of our in vitro studies limits the conclusions that can be drawn. In an effort to more broadly contextualize such findings, we compared our data to selected transcriptomic differences in lung fibroblasts obtained during an in vivo model of fibrosis resolution. We acknowledge that the in vivo and in vitro models differed with respect to the species utilized and the timing of analysis. Additionally, the in vivo data lacked a time point corresponding to peak fibrosis in the young mice, and instead, we compared the data from mice undergoing fibrosis resolution to those from mice with non-resolving fibrosis. Despite these limitations, substantial parallels in the gene signatures of the mesenchymal cells from the two models were apparent and intriguing.

Fibroblasts from mice undergoing the early stages of fibrosis resolution exhibited an anti-proliferative, pro-apoptotic, and anti-adhesion gene signature which resembled that seen in PGE_2- and PGE_2 + FGF2-treated myofibroblasts (Figure 4, A and B, Figure 7A). It is appreciated that mesenchymal cell responses to PGE_2 and/or FGF2 in culture and during fibrosis resolution in vivo may involve the differential behaviors of phenotypically distinct fibroblast subpopulations (74, 75). Moreover, the exclusive use of bulk RNA-seq analysis in both models represents an additional limitation of our study, and single cell approaches as well as flow sorting of isolated fibroblast subpopulations (76) will be necessary in the future to assess the cellular heterogeneity of mesenchymal responses during de-differentiation and fibrosis resolution. Additionally, we acknowledge the importance of confirming these findings in human IPF cells.

Although our study was primarily undertaken to gain a better understanding of the process of myofibroblast de-differentiation, its potential therapeutic ramifications for fibrotic diseases cannot be ignored. Indeed, inhibition of the PGE_2-degrading enzyme 15-PGDH has recently been shown to attenuate lung fibrosis in vivo and to reduce collagen levels in lung slices from IPF patients (77). Our results therefore suggest that, in principal, activation of the cAMP/PKA pathway and MEK/ERK have the potential to lead to fibrosis resolution. Notably,

this raises the possibility that, by blocking FGFR-signaling, the anti-fibrotic drug nintedanib might promote and maintain myofibroblasts, which in turn may limit its therapeutic efficacy. Increasing cAMP can be achieved in variety of ways pharmacologically including treatment with the FDA approved phosphodiesterase inhibitor roflumilast. Pharmacologic strategies to activate ERK are currently under investigation for use as therapeutics in cancer (78, 79). Combined activation of these pathways represents an attractive therapeutic strategy due to their additive effects on myofibroblast de-differentiation with restoration of apoptosis sensitivity. The potential of these approaches require further investigation.

In this study, we have compared – for the first time – the transcriptomic, morphologic, and functional changes in PGE_2- and FGF2-de-differentiated lung myofibroblasts. Although PGE_2- and FGF2-treated myofibroblasts differed in their abilities to proliferate and undergo apoptosis, combined treatment resulted in an anti-proliferative/pro-apoptotic phenotype and an additive effect on de-differentiation. The cell cycle, apoptosis, and focal adhesion gene signatures exhibited by cells from mice undergoing fibrosis resolution more closely resembled those elicited by myofibroblast treatment with PGE_2 than with FGF2, but most closely paralleled the effects of combined PGE_2 + FGF2 treatment in vitro. Mechanistically, PGE_2 induced de-differentiation via cAMP-mediated

deactivation of myofibroblasts, whereas FGF2 utilized MEK/ERK to prompt de-differentiation through myofibroblast proliferation. As neither of the current therapies for IPF exploit cAMP signaling, and as nintedanib antagonizes ERK, our results highlight additional pathways and gene programs that hold promise and warrant further investigation in the development of novel therapeutics for this and other fibrotic diseases.

Methods

Cell Culture

CCL210 normal adult human lung fibroblasts were obtained from the American Type Culture Collection (Manassas, VA). Cell culture was performed in low glucose DMEM (Gibco Invitrogen, Carlsbad, CA) supplemented with 10% FBS (Hyclone, Logan, UT), 100 Units/mL penicillin, and 100 μg/mL streptomycin (Invitrogen). Cells were then serum-starved in FBS-free DMEM overnight and differentiation to myofibroblasts was induced by treatment with TGFβ for 48 h. TGFβ-elicited myofibroblasts were then treated for specified time points as described followed by harvesting (10).

Reagents

Unless otherwise specified, pharmacologic agents were reconstituted in DMSO as stock solutions and stored at -80^{o}C with working concentrations indicated in parentheses. Recombinant human TGFβ (2 ng/mL) and FGF2 (50 ng/mL) were purchased from R&D (Minneapolis, MN) and stored in filter-sterilized 1% BSA at -20^{o}C. Inhibitors of the MAPKs MEK/ERK (PD98059, 20 μM and U0126, 20 μM) and p38 (SB203580, 20 mM) were purchased from Cayman Chemicals (Ann Arbor, MI) and stored at -20^{o}C. PGE_2 (1 μM) purged with nitrogen gas, the E-prostanoid 2

agonist butaprost (500 nM), the direct adenylyl cyclase activator forskolin (500 nM), the JNK inhibitor SP600125 (20 mM), and the AKT-1, -2, -3 inhibitor Triciribine (20 mM) were purchased from Cayman Chemicals. The PKA-selective cAMP agonist 6-BNZ cAMP (2 mM) and the Epac-selective agonist 8-pCPT cAMP (2 mM) were purchased from BioLog (Bremen, Germany) and reconstituted in sterile water. Fast and Power SYBR Green Master Mix and StepOne real time PCR system were procured from Applied Biosystems (Foster City, CA). An αSMA primary antibody conjugated to a FITC-conjugated secondary antibody (Catalog: F3777, Sigma Aldrich, St. Louis, MO), polyclonal annexin V antibody (Catalog: PA5-57231, Thermo Fisher, Waltham, MA), PE-conjugated secondary antibody (Catalog: P2771MP, Thermo Fisher,), and the dyes PKH-26 (Sigma Aldrich) and Prolong™ Gold antifade reagent with DAPI (Invitrogen) were used for immunofluorescence microscopy. Apoptosis was induced with anti-Fas activating antibody (Catalog: CH11, EMD Biosciences, Burlington, MA).

Quantitative Reverse Transcription PCR

Quantitative reverse transcription-PCR (qPCR) analysis of transcript expression was performed by extracting total cellular RNA using an RNeasy kit (Qiagen, Germantown, MD). cDNA was prepared using the High Capacity cDNA Reverse

Transcription Kit (Applied Biosystems), amplified with Fast SYBR Green Master Mix, and analyzed on a StepOne real time PCR system (Applied Biosystems). Fold changes were normalized to the expression levels of the housekeeping gene GAPDH. Primer pair sequences used for qPCR are listed in Supplemental Table 6.

Western Blot

For Western blot analysis, cells were lysed in RIPA buffer supplemented with protease inhibitors (Roche Diagnostics, Indianapolis, IN) and a phosphatase inhibitor cocktail (EMD Biosciences). Proteins were separated by SDS-PAGE and transferred to a nitrocellulose membrane. Membranes were subsequently blocked with 5% nonfat dry milk or 5% BSA and probed with a mouse antibody specific to αSMA at 1:2000 (Catalog: ab7817, Abcam, Cambridge, MA) or the rabbit antibodies targeting caspase-3 (CASP3, Catalog: #9662S), poly (ADP-ribose) polymerase (PARP, Catalog: #9532S), and GAPDH HRP conjugate (Catalog: #8884S) at 1:1000 (Cell Signaling Technologies, Danvers, MA). All experiments were performed in triplicate and the results presented as mean ± SEM.

Immunofluorescence Microscopy

CCL210 fibroblasts were seeded and cultured in single-chamber slides (Nunc, Rochester, NY) followed by overnight serum starvation. Myofibroblasts were generated by incubation with TGFβ for 48 h and then treated with PGE_2 and/or FGF2 for an additional 5 d. Chamber slides were then washed twice with chilled PBS, fixed with freshly prepared 4% formaldehyde for 20 min, washed with PBS and quenched with 100 mM glycine for 15 min. Blocking and permeabilization were achieved by incubating the slides for 1 h in PBS containing 10% FBS and 0.1% Triton X100. Cells were then incubated with either anti-αSMA-FITC (1:500) overnight at 4°C, anti-annexin V (1 μg/mL) at 37°C for 1 h followed by anti-rabbit PE conjugated secondary antibody overnight at 4°C, or the membrane dye PKH26 (2 μM) at RT for 3 min. Mounting medium containing DAPI was then used to stain the nuclei. Slides were examined using a Leica DC 500-fluorescence microscope equipped with a digital camera.

Proliferation and Apoptosis Assays

Lung myofibroblast proliferation studies were performed using the CyQUANT NF Cell Proliferation Assay Kit (Thermo Fisher). At the specified harvesting time, cells were detached with 0.25% trypsin, and re-suspended in Hank's Balanced Salt Solution containing CyQUANT NF dye reagent. Cell lysates were then transferred

to a 96-well plate and incubated at 37^{o}C for 45 min. Cell proliferation was measured by determining fluorescence in a microplate reader with excitation of 485 nm and emission of 530 nm. Lung myofibroblast apoptosis was evaluated following treatment with anti-Fas antibody at 100 ng/mL. Total and cleaved (active) forms of CASP3 and PARP were analyzed by Western blot. All experiments were performed in triplicate and the results presented as mean ± SEM.

RNA-seq

For RNA-seq performed on in vitro specimens, CCL210 human adult lung fibroblasts were treated with PGE_2, FGF2, or left untreated. Cells were harvested with Trizol followed by RNA extraction using the miRNeasy Mini kit (Qiagen) according to the manufacturer's protocol and submitted for library prep and sequencing. For RNA-seq performed on fibroblasts from an in vivo model of fibrosis resolution, young (2 mo) and aged (18 mo) female (FVB strain) Col1α1-GFP transgenic mice were treated with bleomycin and sacrificed on day 30 (80). Mouse lungs were digested and Col1α1-GFP+ fibroblasts were isolated by FACS sorting. Total RNA was extracted using the RNeasy Micro Kit (Qiagen) according to manufacturer's protocol and submitted for library prep and sequencing. A

detailed description of RNA library preparation, sequencing protocols, and analysis of RNA isolated from CCL210 and mouse fibroblasts is available in the supplement. Our RNA-Seq data was deposited in the NCBI GEO database (accession GSE163832).

Statistics

Statistical analysis was performed using GraphPad Prism software version 8.1.1. Experimental data are presented as means and were analyzed for statistical significance by one-way ANOVA with the Tukey's multiple comparisons test, two-way ANOVA (Figure 6B), or paired t-test, as appropriate. A cutoff *P*-value of <0.05 was considered significant. Error bars represent SEM. For RNA-seq data, DESeq2 was used with default parameters to identify differentially expressed transcripts with cutoffs of Benjamini-Hochberg FDR (0.05) adjusted *P*-values < 0.05 and fold-change values (excluding small RNAs) of < -1.5 or > 1.5 (81). We elected to omit fold-change cutoffs when analyzing small RNAs to capture all statistically significant changes that may have biologic relevance. Functional analysis of all RNAs (except small RNAs), including candidate pathways activated or inhibited in comparison(s) and GO-term enrichments (http://www.geneontology.org/), was

performed using iPathway Guide (http://www.advaitabio.com) (82). See supplement for detailed quality control and sequence alignment methodology.

Study Approval

All animal experiments were carried out in accordance with the Mayo Clinic Institutional Animal Care and Use Committee (IACUC) and conforming to the ARRIVE guidelines.

References

1. Wynn TA. Fibrotic disease and the T(H)1/T(H)2 paradigm. *Nat Rev Immunol*. Aug 2004;4(8):583-94.

2. Wynn TA. Cellular and molecular mechanisms of fibrosis. *J Pathol*. Jan 2008;214(2):199-210.

3. Fell CD, et al. Clinical predictors of a diagnosis of idiopathic pulmonary fibrosis. *Am J Respir Crit Care Med*. Apr 15 2010;181(8):832-7.

4. Vaughan MB, et al. Transforming growth factor-beta1 promotes the morphological and functional differentiation of the myofibroblast. *Exp Cell Res*. May 25 2000;257(1):180-9.

5. Penke LR, Peters-Golden M. Molecular determinants of mesenchymal cell activation in fibroproliferative diseases. *Cell Mol Life Sci*. Nov 2019;76(21):4179-4201.

6. Thannickal VJ, Horowitz JC. Evolving concepts of apoptosis in idiopathic pulmonary fibrosis. *Proc Am Thorac Soc*. Jun 2006;3(4):350-6.

7. Hinz B, Lagares D. Evasion of apoptosis by myofibroblasts: a hallmark of fibrotic diseases. *Nat Rev Rheumatol*. Jan 2020;16(1):11-31.

8. Horowitz JC, Thannickal VJ. Mechanisms for the Resolution of Organ Fibrosis. *Physiology (Bethesda)*. Jan 1 2019;34(1):43-55.

9. Kato K, et al. Impaired Myofibroblast Dedifferentiation Contributes to Non-Resolving Fibrosis in Aging. *Am J Respir Cell Mol Biol*. Jan 21 2020;

10. Garrison G, et al. Reversal of myofibroblast differentiation by prostaglandin E(2). *Am J Respir Cell Mol Biol*. May 2013;48(5):550-8.

11. Huang S, et al. Prostaglandin E(2) inhibits collagen expression and proliferation in patient-derived normal lung fibroblasts via E prostanoid 2 receptor and cAMP signaling. *Am J Physiol Lung Cell Mol Physiol*. Feb 2007;292(2):L405-13.

12. Wettlaufer SH, et al. Reversal of the Transcriptome by Prostaglandin E2 during Myofibroblast Dedifferentiation. *Am J Respir Cell Mol Biol*. Jan 2016;54(1):114-27.

13. Maltseva O, et al. Fibroblast growth factor reversal of the corneal myofibroblast phenotype. *Invest Ophthalmol Vis Sci*. Oct 2001;42(11):2490-5.

14. Koo HY, et al. Fibroblast growth factor 2 decreases bleomycin-induced pulmonary fibrosis and inhibits fibroblast collagen production and myofibroblast differentiation. *J Pathol*. Sep 2018;246(1):54-66.

15. Narumiya S, et al. Prostanoid receptors: structures, properties, and functions. *Physiol Rev*. Oct 1999;79(4):1193-226.

16. Ornitz DM, Itoh N. The Fibroblast Growth Factor signaling pathway. *Wiley Interdiscip Rev Dev Biol*. May-Jun 2015;4(3):215-66.

17. Penke LR, et al. Prostaglandin E2 inhibits alpha-smooth muscle actin transcription during myofibroblast differentiation via distinct mechanisms of modulation of serum response factor and myocardin-related transcription factor-A. *J Biol Chem*. Jun 13 2014;289(24):17151-62.

18. Wettlaufer SH, et al. Distinct PKA regulatory subunits mediate PGE2 inhibition of TGFbeta-1-stimulated collagen I translation and myofibroblast differentiation. *Am J Physiol Lung Cell Mol Physiol*. Oct 1 2017;313(4):L722-l731.

19. Kolodsick JE, et al. Prostaglandin E2 inhibits fibroblast to myofibroblast transition via E. prostanoid receptor 2 signaling and cyclic adenosine monophosphate elevation. *Am J Respir Cell Mol Biol*. Nov 2003;29(5):537-44.

20. Stepp MW, et al. The c10orf10 gene product is a new link between oxidative stress and autophagy. *Biochim Biophys Acta*. Jun 2014;1843(6):1076-88.

21. Yoshida K, et al. MAP kinase activation and apoptosis in lung tissues from patients with idiopathic pulmonary fibrosis. *J Pathol*. Nov 2002;198(3):388-96.

22. Nho RS, Hergert P. IPF fibroblasts are desensitized to type I collagen matrix-induced cell death by suppressing low autophagy via aberrant Akt/mTOR kinases. *PLoS One*. 2014;9(4):e94616.

23. Lawrence J, Nho R. The Role of the Mammalian Target of Rapamycin (mTOR) in Pulmonary Fibrosis. *Int J Mol Sci*. Mar 8 2018;19(3)

24. Khalil N, Greenberg AH. The role of TGF-beta in pulmonary fibrosis. *Ciba Found Symp*. 1991;157:194-207; discussion 207-11.

25. Yue X, et al. TGF-β: Titan of Lung Fibrogenesis. *Curr Enzym Inhib*. Jul 1 2010;6(2)

26. Fernandez IE, Eickelberg O. The impact of TGF-beta on lung fibrosis: from targeting to biomarkers. *Proc Am Thorac Soc*. Jul 2012;9(3):111-6.

27. Hecker L, et al. NADPH oxidase-4 mediates myofibroblast activation and fibrogenic responses to lung injury. *Nat Med*. Sep 2009;15(9):1077-81.

28. Wernig G, et al. Unifying mechanism for different fibrotic diseases. *Proc Natl Acad Sci U S A*. May 2 2017;114(18):4757-4762.

29. Eferl R, et al. Development of pulmonary fibrosis through a pathway involving the transcription factor Fra-2/AP-1. *Proc Natl Acad Sci U S A*. Jul 29 2008;105(30):10525-30.

30. Crestani B, et al. Hepatocyte growth factor and lung fibrosis. *Proc Am Thorac Soc*. Jul 2012;9(3):158-63.

31. Marchand-Adam S, et al. Defect of hepatocyte growth factor secretion by fibroblasts in idiopathic pulmonary fibrosis. *Am J Respir Crit Care Med*. Nov 15 2003;168(10):1156-61.

32. Schaller MD. Cellular functions of FAK kinases: insight into molecular mechanisms and novel functions. *J Cell Sci*. Apr 1 2010;123(Pt 7):1007-13.

33. Hecker L, et al. Reversible differentiation of myofibroblasts by MyoD. *Exp Cell Res*. Aug 1 2011;317(13):1914-21.

34. Penke LR, et al. FOXM1 is a critical driver of lung fibroblast activation and fibrogenesis. *J Clin Invest*. Jun 1 2018;128(6):2389-2405.

35. Huang SK, et al. Prostaglandin E2 inhibits specific lung fibroblast functions via selective actions of PKA and Epac-1. *Am J Respir Cell Mol Biol*. Oct 2008;39(4):482-9.

36. Lama V, et al. Prostaglandin E2 synthesis and suppression of fibroblast proliferation by alveolar epithelial cells is cyclooxygenase-2-dependent. *Am J Respir Cell Mol Biol*. Dec 2002;27(6):752-8.

37. Huang WT, et al. Plasminogen activator inhibitor 1, fibroblast apoptosis resistance, and aging-related susceptibility to lung fibrosis. *Exp Gerontol*. Jan 2015;61:62-75.

38. Esteller M. Non-coding RNAs in human disease. *Nat Rev Genet*. Nov 18 2011;12(12):861-74.

39. O'Reilly S. MicroRNAs in fibrosis: opportunities and challenges. *Arthritis Res Ther*. Jan 13 2016;18:11.

40. Pandit KV, Milosevic J. MicroRNA regulatory networks in idiopathic pulmonary fibrosis. *Biochem Cell Biol*. Apr 2015;93(2):129-37.

41. Hadjicharalambous MR, Lindsay MA. Idiopathic Pulmonary Fibrosis: Pathogenesis and the Emerging Role of Long Non-Coding RNAs. *Int J Mol Sci*. Jan 14 2020;21(2)

42. Yu F, et al. NEAT1 accelerates the progression of liver fibrosis via regulation of microRNA-122 and Kruppel-like factor 6. *J Mol Med (Berl)*. Nov 2017;95(11):1191-1202.

43. Huang S, et al. Long noncoding RNA MALAT1 mediates cardiac fibrosis in experimental postinfarct myocardium mice model. *J Cell Physiol*. Mar 2019;234(3):2997-3006.

44. Savary G, et al. The Long Noncoding RNA DNM3OS Is a Reservoir of FibromiRs with Major Functions in Lung Fibroblast Response to TGF-beta and Pulmonary Fibrosis. *Am J Respir Crit Care Med*. Jul 15 2019;200(2):184-198.

45. Huang C, et al. Long Noncoding RNA FENDRR Exhibits Antifibrotic Activity in Pulmonary Fibrosis. *Am J Respir Cell Mol Biol*. Apr 2020;62(4):440-453.

46. Ouyang F, et al. Long non-coding RNA RNF7 promotes the cardiac fibrosis in rat model via miR-543/THBS1 axis and TGFbeta1 activation. *Aging (Albany NY)*. Jan 8 2020;12(1):996-1010.

47. Othman N, Nagoor NH. The role of microRNAs in the regulation of apoptosis in lung cancer and its application in cancer treatment. *Biomed Res Int*. 2014;2014:318030.

48. Gao Q, et al. Antifibrotic Potential of MiR-335-3p in Hereditary Gingival Fibromatosis. *J Dent Res*. Sep 2019;98(10):1140-1149.

49. Nakashima T, et al. Impaired IL-17 signaling pathway contributes to the increased collagen expression in scleroderma fibroblasts. *J Immunol*. Apr 15 2012;188(8):3573-83.

50. Pang Q, et al. MicroRNA-152-5p inhibits proliferation and migration and promotes apoptosis by regulating expression of Smad3 in human keloid fibroblasts. *BMB Rep*. Mar 2019;52(3):202-207.

51. Zhang Y, et al. let-7a suppresses liver fibrosis via TGFbeta/SMAD signaling transduction pathway. *Exp Ther Med*. May 2019;17(5):3935-3942.

52. Yang S, et al. miR-145 regulates myofibroblast differentiation and lung fibrosis. *Faseb j*. Jun 2013;27(6):2382-91.

53. Huang Y, et al. MicroRNA-21: a central regulator of fibrotic diseases via various targets. *Curr Pharm Des*. 2015;21(17):2236-42.

54. Cui H, et al. MicroRNA-27a-3p Is a Negative Regulator of Lung Fibrosis by Targeting Myofibroblast Differentiation. *Am J Respir Cell Mol Biol*. Jun 2016;54(6):843-52.

55. Salmena L, et al. A ceRNA hypothesis: the Rosetta Stone of a hidden RNA language? *Cell*. Aug 5 2011;146(3):353-8.

56. Li P, et al. Cytochrome c and dATP-dependent formation of Apaf-1/caspase-9 complex initiates an apoptotic protease cascade. *Cell*. Nov 14 1997;91(4):479-89.

57. Moore BB, et al. Animal models of fibrotic lung disease. *Am J Respir Cell Mol Biol*. Aug 2013;49(2):167-79.

58. Cabrera S, et al. Delayed resolution of bleomycin-induced pulmonary fibrosis in absence of MMP13 (collagenase 3). *Am J Physiol Lung Cell Mol Physiol*. May 1 2019;316(5):L961-l976.

59. Caporarello N, et al. Vascular dysfunction in aged mice contributes to persistent lung fibrosis. *Aging Cell*. Jul 21 2020:e13196.

60. Grosse R, et al. A role for VASP in RhoA-Diaphanous signalling to actin dynamics and SRF activity. *Embo j*. Jun 16 2003;22(12):3050-61.

61. Jin J, et al. Pirfenidone attenuates lung fibrotic fibroblast responses to transforming growth factor-β1. *Respir Res*. Jun 11 2019;20(1):119.

62. Wolters PJ, et al. Pathogenesis of idiopathic pulmonary fibrosis. *Annu Rev Pathol*. 2014;9:157-79.

63. Zmajkovicova K, et al. The Antifibrotic Activity of Prostacyclin Receptor Agonism Is Mediated through Inhibition of YAP/TAZ. *Am J Respir Cell Mol Biol*. May 2019;60(5):578-591.

64. Emelyanova L, et al. Impact of statins on cellular respiration and de-differentiation of myofibroblasts in human failing hearts. *ESC Heart Fail*. Oct 2019;6(5):1027-1040.

65. Suzuki K, et al. Transcriptomic changes involved in the dedifferentiation of myofibroblasts derived from the lung of a patient with idiopathic pulmonary fibrosis. *Mol Med Rep*. Aug 2020;22(2):1518-1526.

66. Micallef L, et al. The myofibroblast, multiple origins for major roles in normal and pathological tissue repair. *Fibrogenesis Tissue Repair*. 2012;5(Suppl 1):S5.

67. Schafer MJ, et al. Cellular senescence mediates fibrotic pulmonary disease. *Nat Commun*. Feb 23 2017;8:14532.

68. Thannickal VJ, et al. Myofibroblast differentiation by transforming growth factor-beta1 is dependent on cell adhesion and integrin signaling via focal adhesion kinase. *J Biol Chem*. Apr 4 2003;278(14):12384-9.

69. Thomas PE, et al. PGE(2) inhibition of TGF-beta1-induced myofibroblast differentiation is Smad-independent but involves cell shape and adhesion-dependent signaling. *Am J Physiol Lung Cell Mol Physiol*. Aug 2007;293(2):L417-28.

70. Kopp F, Mendell JT. Functional Classification and Experimental Dissection of Long Noncoding RNAs. *Cell*. Jan 25 2018;172(3):393-407.

71. Ebert MS, Sharp PA. Roles for microRNAs in conferring robustness to biological processes. *Cell*. Apr 27 2012;149(3):515-24.

72. Bozyk PD, Moore BB. Prostaglandin E2 and the pathogenesis of pulmonary fibrosis. *Am J Respir Cell Mol Biol*. Sep 2011;45(3):445-52.

73. Guzy RD, et al. Fibroblast growth factor 2 is required for epithelial recovery, but not for pulmonary fibrosis, in response to bleomycin. *Am J Respir Cell Mol Biol*. Jan 2015;52(1):116-28.

74. Lee JH, et al. Anatomically and Functionally Distinct Lung Mesenchymal Populations Marked by Lgr5 and Lgr6. *Cell*. Sep 7 2017;170(6):1149-1163.e12.

75. Habiel DM, Hogaboam CM. Heterogeneity of Fibroblasts and Myofibroblasts in Pulmonary Fibrosis. *Curr Pathobiol Rep*. Jun 2017;5(2):101-110.

76. Zepp JA, et al. Distinct Mesenchymal Lineages and Niches Promote Epithelial Self-Renewal and Myofibrogenesis in the Lung. *Cell*. Sep 7 2017;170(6):1134-1148.e10.

77. Bärnthaler T, et al. Inhibiting eicosanoid degradation exerts antifibrotic effects in a pulmonary fibrosis mouse model and human tissue. *J Allergy Clin Immunol*. Mar 2020;145(3):818-833.e11.

78. Andersson CR, et al. Mebendazole is unique among tubulin-active drugs in activating the MEK–ERK pathway. *Scientific Reports*. 2020/08/04 2020;10(1):13124.

79. Guerini AE, et al. Mebendazole as a Candidate for Drug Repurposing in Oncology: An Extensive Review of Current Literature. *Cancers (Basel)*. Aug 31 2019;11(9)

80. Caporarello N, et al. PGC1α repression in IPF fibroblasts drives a pathologic metabolic, secretory and fibrogenic state. *Thorax*. Aug 2019;74(8):749-760.

81. Love MI, et al. Moderated estimation of fold change and dispersion for RNA-seq data with DESeq2. *Genome Biol*. 2014;15(12):550.

82. Draghici S, et al. A systems biology approach for pathway level analysis. *Genome Res*. Oct 2007;17(10):1537-45.

83. Chen Q, et al. Long non-coding RNA PCAT-1 promotes cardiac fibroblast proliferation via upregulating TGF-beta1. *Eur Rev Med Pharmacol Sci*. Dec 2019;23(23):10517-10522.

84. Xu W, et al. Long non-coding RNA PCAT-1 contributes to tumorigenesis by regulating FSCN1 via miR-145-5p in prostate cancer. *Biomed Pharmacother*. Nov 2017;95:1112-1118.

85. Shang AQ, et al. Knockdown of long noncoding RNA PVT1 suppresses cell proliferation and invasion of colorectal cancer via upregulation of microRNA-214-3p. *Am J Physiol Gastrointest Liver Physiol*. Aug 1 2019;317(2):G222-g232.

86. Tang PM, et al. LncRNAs in TGF-β-Driven Tissue Fibrosis. *Noncoding RNA*. Oct 4 2018;4(4)

87. Jiang X, et al. LncRNA NEAT1 promotes hypoxia-induced renal tubular epithelial apoptosis through downregulating miR-27a-3p. *J Cell Biochem*. Sep 2019;120(9):16273-16282.

88. Liao K, et al. Blocking lncRNA MALAT1/miR-199a/ZHX1 Axis Inhibits Glioblastoma Proliferation and Progression. *Mol Ther Nucleic Acids*. Dec 6 2019;18:388-399.

89. Han Y, et al. Hsa-miR-125b suppresses bladder cancer development by down-regulating oncogene SIRT7 and oncogenic long noncoding RNA MALAT1. *FEBS Lett*. Oct 25 2013;

90. Wang P, et al. LncRNA MEG3 enhances cisplatin sensitivity in non-small cell lung cancer by regulating miR-21-5p/SOX7 axis. *Onco Targets Ther*. 2017;10:5137-5149.

91. Braconi C, et al. microRNA-29 can regulate expression of the long non-coding RNA gene MEG3 in hepatocellular cancer. *Oncogene*. Nov 24 2011;30(47):4750-6.

92. Tang R, et al. LncRNA GAS5 attenuates fibroblast activation through inhibiting Smad3 signaling. *Am J Physiol Cell Physiol*. Jul 1 2020;319(1):C105-c115.

Author contributions

S.M.F., L.R.P, and M.P-G designed the in vitro experiments. T.X.P. and G.L. designed the in vivo experiments. Experiments were performed by S.M.F., L.R.P., and T.X.P. Data were analyzed by S.M.F. and D.K. The manuscript was written by S.M.F. and M.P-G.

Acknowledgments

We thank members of the Peters-Golden and Steven Huang labs for their valuable input into this work. We acknowledge support from the Bioinformatics Core of the University of Michigan Medical School's Biomedical Research Core Facilities and specifically thank Becky Tagett for her work on the small RNA sequencing and analysis. This work was funded by the NIH grants RO1 HL094311 (to M.P-G), R35 HL144979 (to M.P-G.), HL142596 (to G.L.), and 5T32HL007749-28 (to S.M.F.).

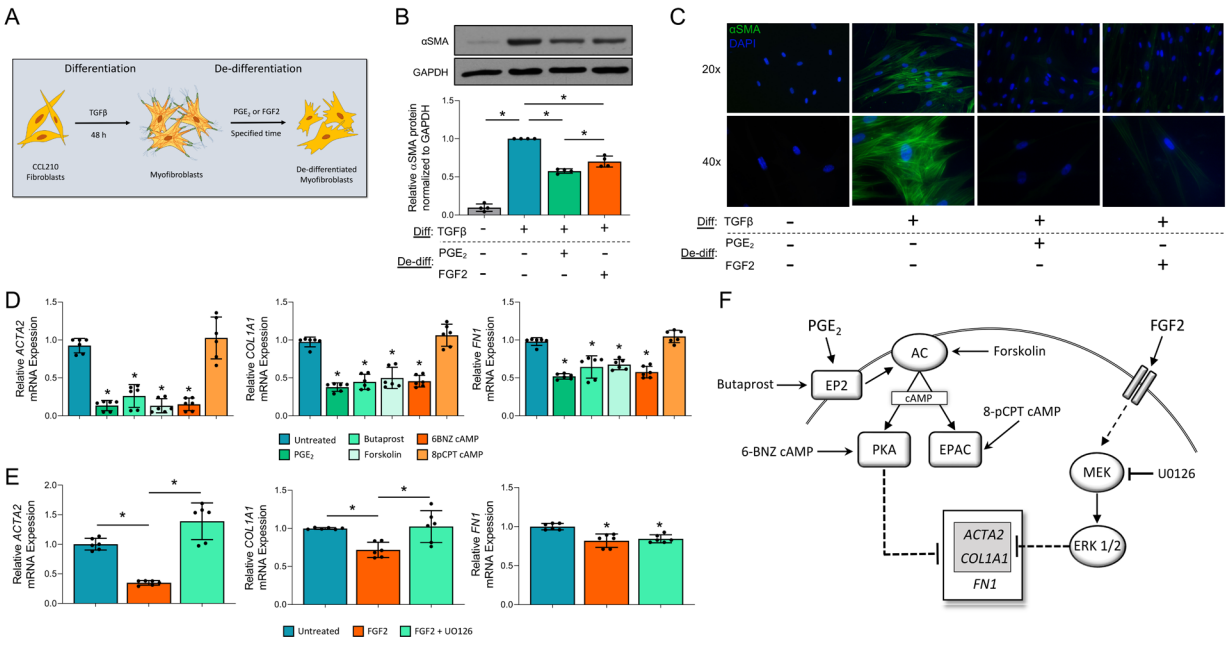

Figure 1. PGE_2 and FGF2 de-differentiate established myofibroblasts via distinct signaling pathways. (**A**) Experimental scheme depicting myofibroblast differentiation of CCL210 fibroblasts with TGFβ (2 ng/mL) for 48 h followed by de-differentiation with PGE_2 (1 μM) or FGF2 (50 ng/mL). (**B**) αSMA protein expression measured by Western blot analysis 5 d following treatment with PGE_2 or FGF2 compared to untreated fibroblast and myofibroblast controls. The histogram depicts mean densitometry values. (**C**) αSMA stress fibers identified by immunofluorescence microscopy using anti-αSMA antibody and FITC-conjugated secondary antibody. Nuclei are stained with DAPI. (**D**) Relative *ACTA2*, *COL1A1*,

and *FN1* expression by qPCR in myofibroblasts treated for 24 h with PGE_2 (1 µM), the EP2 agonist butaprost (500 nM), the adenylate cyclase activator forskolin (500 nM), the PKA specific cAMP analog 6-BNZ cAMP (2 mM), or the Epac specific cAMP analog 8-pCPT cAMP (2 mM). (**E**) Relative *ACTA2*, *COL1A1*, and *FN1* expression by qPCR in myofibroblasts treated for 48 h with FGF2 (50 ng/mL) with and without the MEK/ERK inhibitor UO126 (20 µM). (**F**) Schematic detailing PGE_2 signaling cascade via the EP2 receptor and FGF2 signaling through FGF2R via MEK/ERK. PKA mediates the reduction in *ACTA2*, *COL1A1*, and *FN1* elicited by PGE_2 while MEK/ERK mediates the reduction in *ACTA2*, *COL1A1* elicited by FGF2. Relative fold changes of indicated genes measured by qPCR are normalized to *GAPDH*. Bars represent mean ± SEM. Data points in (**B**) represent individual replicate samples from four separate experiments. Data points in (**D**) and (**E**) represent paired replicate samples from three experiments. Lines indicate conditions being compared. An isolated asterisk indicates statistical significance compared with untreated myofibroblast. $*P < 0.05$, one-way ANNOVA. Diff = Differentiation; De-diff = De-differentiation. AC = adenylate cyclase.

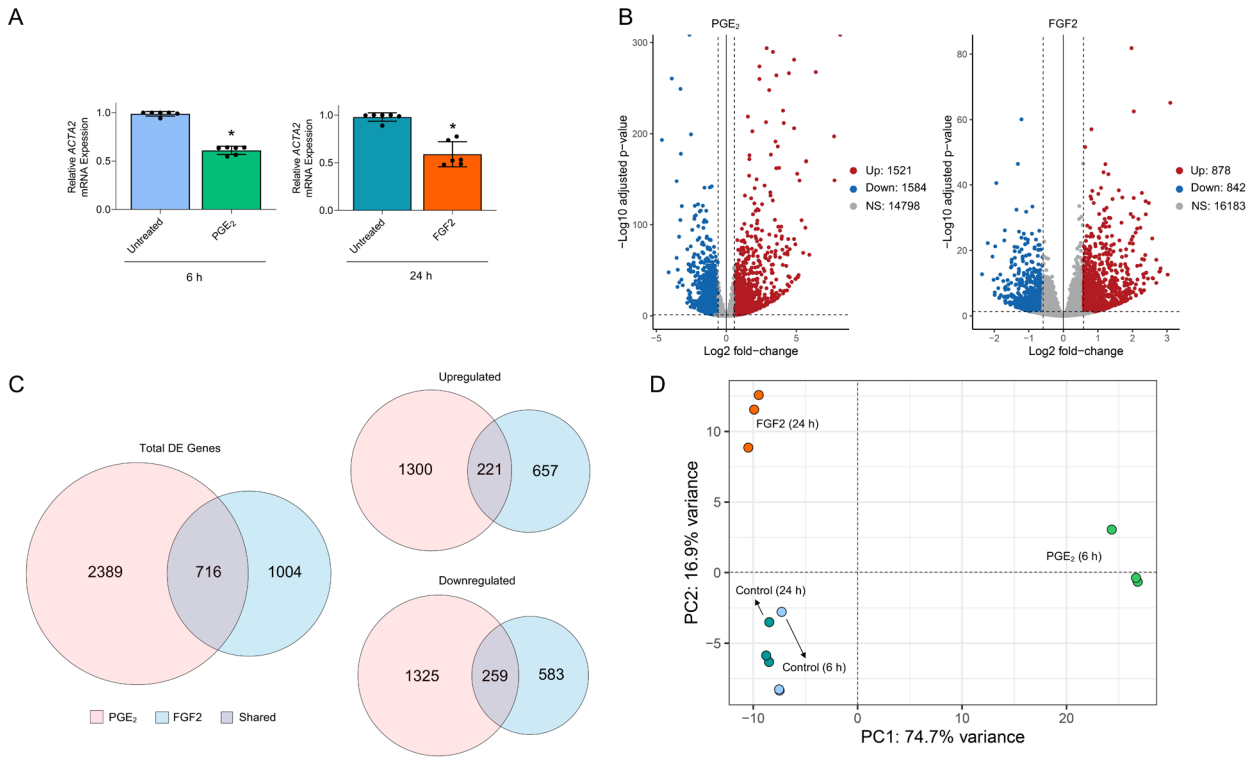

Figure 2. RNA-seq of established myofibroblasts treated with or without PGE_2 or FGF2. (**A**) qPCR analysis of RNA samples submitted for RNA-seq demonstrating ~50% reduction in *ACTA2* expression in myofibroblasts treated with PGE_2 (1 µM) or FGF2 (50 ng/mL) at 6 and 24 h, respectively. Data points represent paired replicate samples from three experiments. Bars represent mean ± SEM. **P* < 0.05, paired t-test. (**B**) Volcano plots representing differential gene expression by log2 fold change (x-axis) and adjusted *P*-value (y-axis) of total RNA transcripts in PGE_2- and FGF2-treated myofibroblasts compared to time-matched controls. (**C**) Venn diagrams depicting the number of genes differentially expressed as well as

those specifically upregulated and downregulated exclusively by PGE_2 (red), exclusively by FGF2 (blue), and by both mediators (grey). (**D**) Principal components analysis of the top 500 variably expressed genes in PGE_2- and FGF2-treated myofibroblasts and untreated time-matched controls. Relative fold changes of indicated genes measured by qPCR are normalized to *GAPDH*. Each colored circle denotes one of three replicate samples.

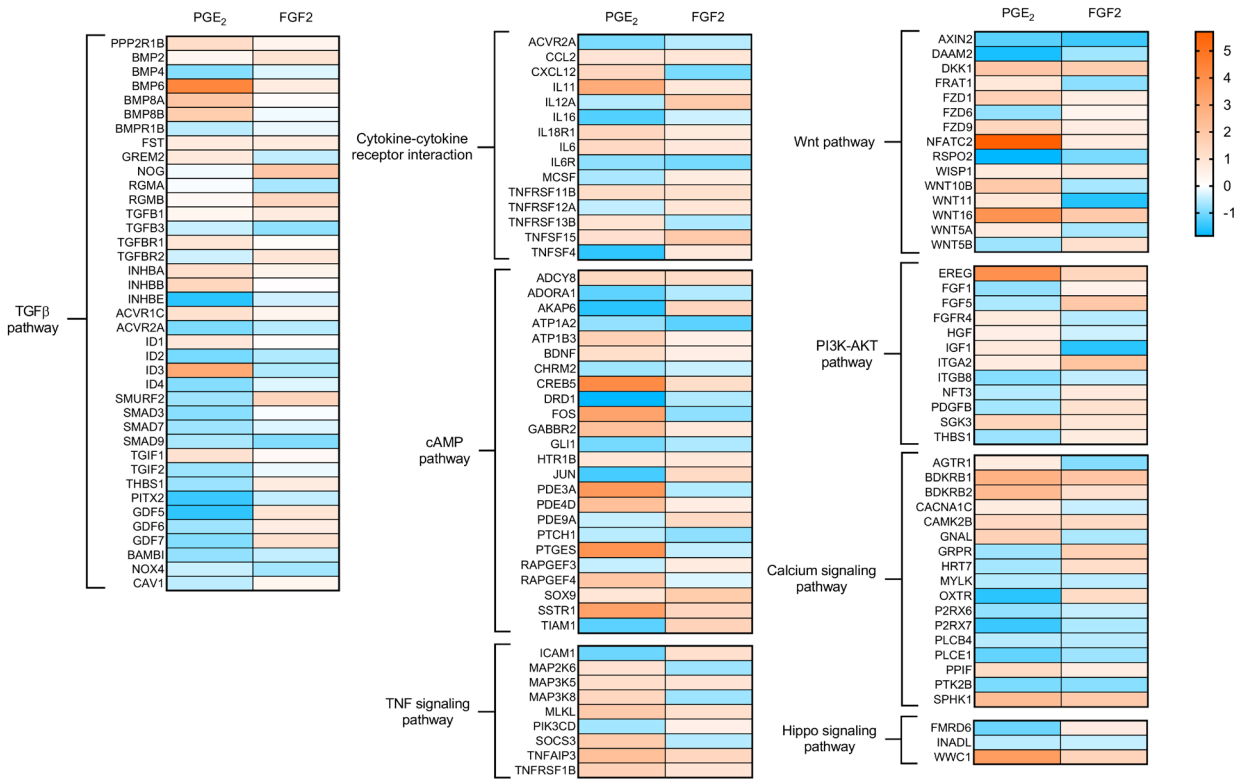

Figure 3. Regulation of genes from KEGG pathways enriched by both PGE_2 and FGF2. Heatmap display of individual genes belonging to the specified pathways in myofibroblasts treated with PGE_2 or FGF2 for 6 and 24 h, respectively. Color scale depicts range of log2 fold changes in gene expression.

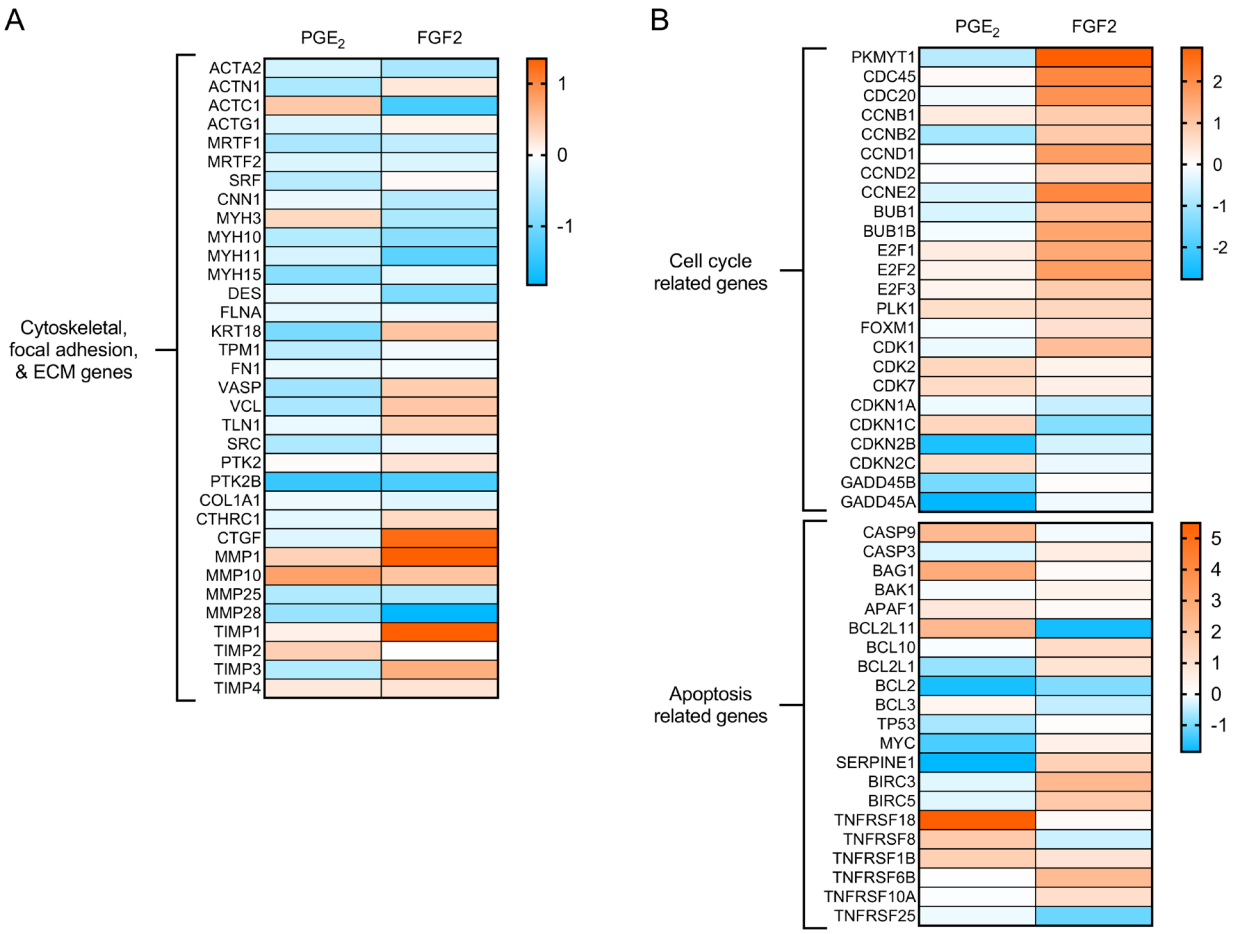

Figure 4. Gene ontology characteristics of myofibroblasts following treatment with PGE_2 or FGF2. Heatmap display of (**A**) cytoskeletal, ECM-related, and focal adhesion, (**B**) cell cycle and apoptosis genes in PGE_2 - and FGF2-treated myofibroblasts compared to 6 and 24 h time-matched controls. Color scale depicts range of log2 fold changes in gene expression. ECM = extracellular matrix.

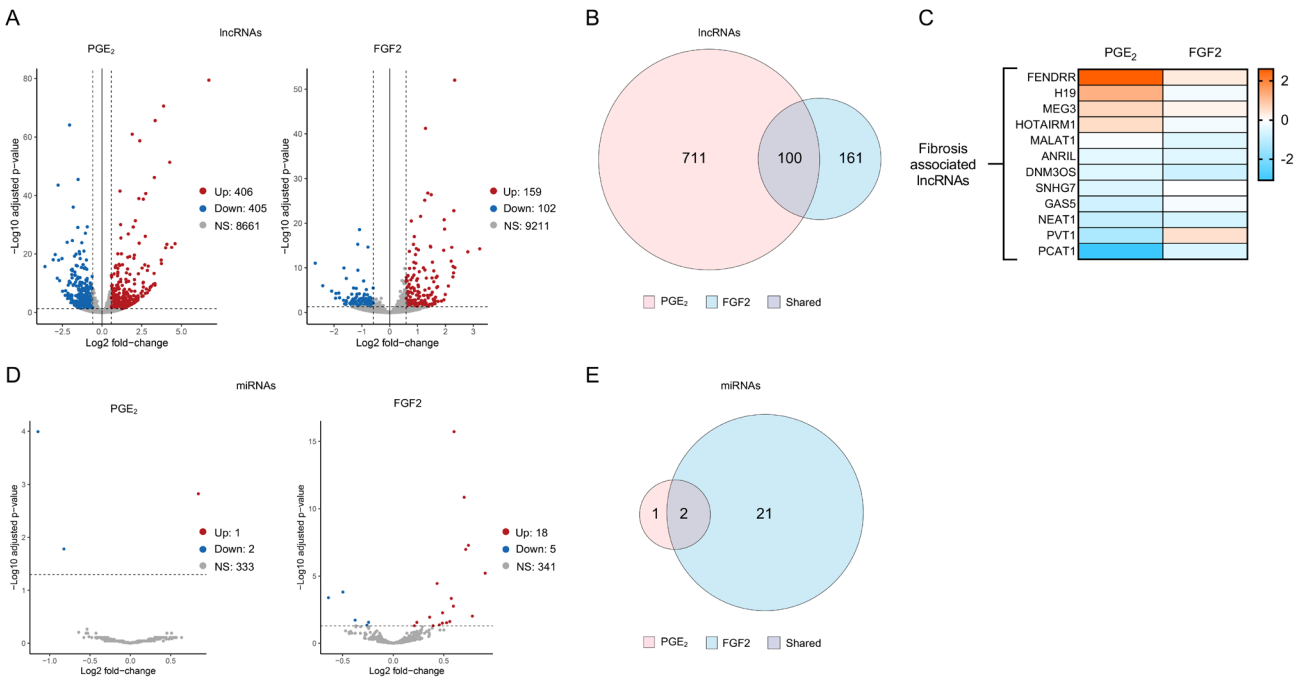

Figure 5. PGE_2 and FGF2 modulate the expression of fibrosis-associated long non-coding RNAs and miRNAs in myofibroblasts. Volcano plots representing differential (**A**) lncRNA expression and (**D**) miRNA expression by log2 fold change (x-axis) and adjusted *P*-value (y-axis) of total RNA transcripts in PGE_2- and FGF2-treated myofibroblasts compared to time-matched controls. Threshold for lncRNAs set by log2 fold change -0.5 to 0.5 and adjusted *P*-value <0.05. Threshold for miRNAs set by adjusted *P*-value <0.05 only. Venn diagrams depicting the number of differentially expressed (**B**) lncRNAs and (**E**) miRNAs exclusively by

PGE_2 (red), exclusively by FGF2 (blue), and by both mediators (grey). (**C**) Heatmap display of fibrosis-associated lncRNAs differentially regulated by PGE_2 and/or FGF2. Color scale depicts range of log2 fold changes in gene expression.

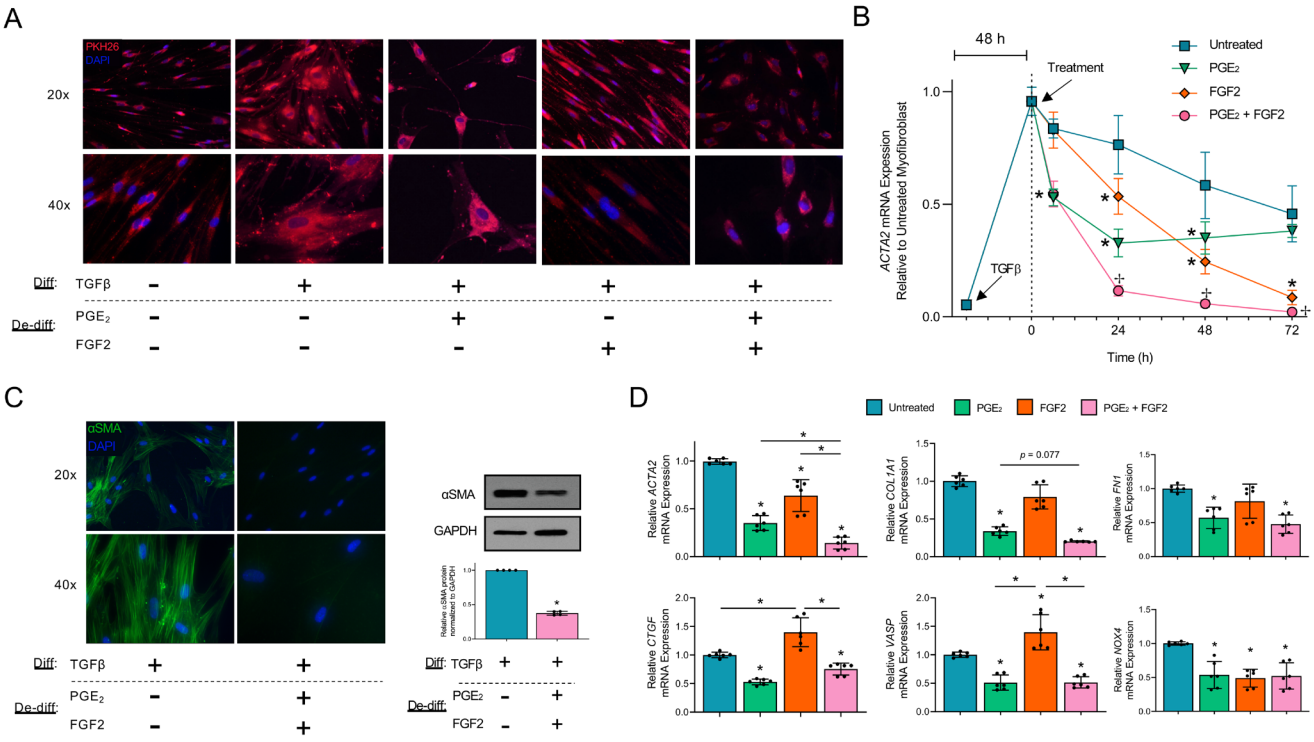

Figure 6. Myofibroblasts treated with PGE_2 and FGF2 separately or in combination produce distinct cellular morphologies and fibrosis-associated gene expression patterns. CCL210 fibroblasts were differentiated to myofibroblasts with TGFβ (2 ng/mL) and treated with PGE_2 (1 μM), FGF2 (50 ng/mL), or both. (**A**) Cells were stained with the membrane dye PKH26 (2 μM) and examined by fluorescence microscopy 5 d after treatment. (**B**) Kinetics of *ACTA2* in untreated, PGE_2-, FGF2-, and PGE_2 + FGF2-treated myofibroblasts. Fibroblasts were treated with TGFβ for 48 h followed by treatment and harvesting for mRNA at the

indicated time points. (**C**) Immunofluorescence microscopy and representative Western blot for αSMA in untreated and PGE_2 + FGF2-treated myofibroblasts evaluated at 5 d. The histogram depicts mean densitometry values. (**D**) qPCR analysis of the fibrosis-associated genes *ACTA2, COL1A1, FN1, CTGF, VASP,* and *NOX4* after 24 h of PGE_2 ± FGF2 compared to untreated myofibroblast control. Relative fold changes of indicated genes measured by qPCR are normalized to *GAPDH*. Bars represent mean ± SEM; data points represent replicate samples from three experiments. Lines indicate conditions being compared. Isolated asterisks indicate statistical significance compared with untreated myofibroblast; spoked asterisk "✢" in (**B**) indicate statistical significance compared with untreated, PGE_2-, and FGF2-treated myofibroblasts. * and ✢ $P < 0.05$. Performed two-way ANNOVA for (**B**), paired t-test for (**C**), and one-way ANNOVA for (**D**). Diff = Differentiation; De-diff = De-differentiation.

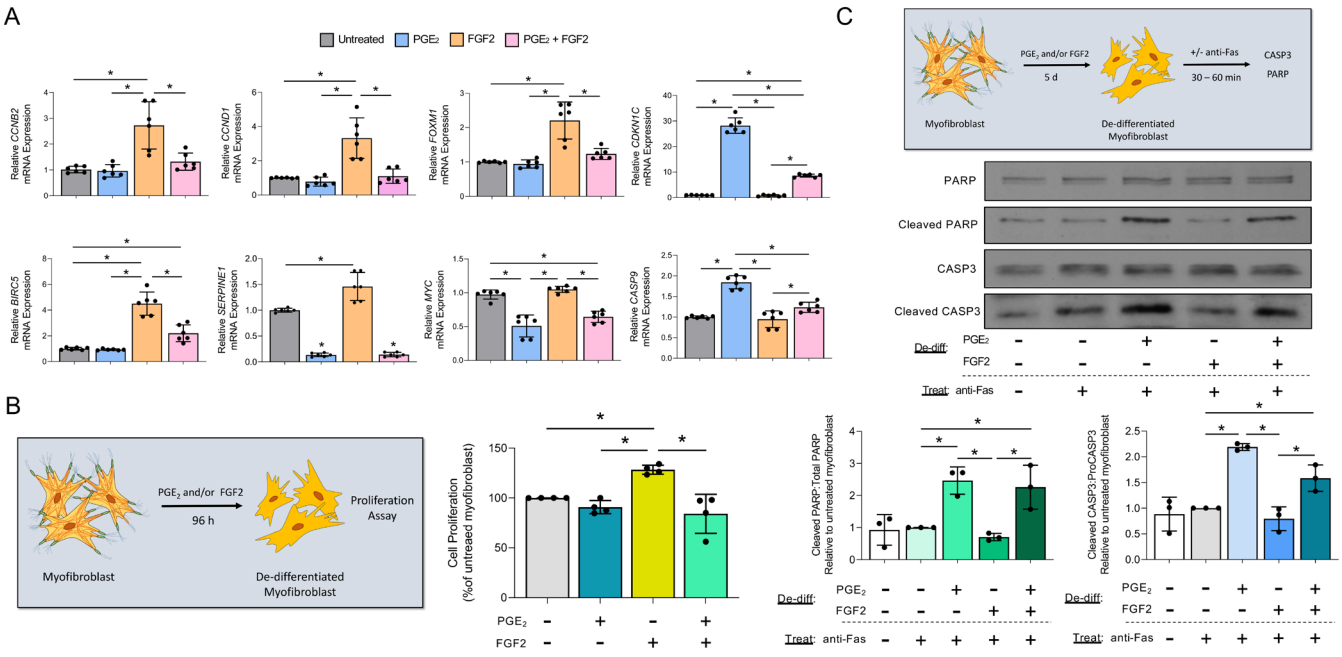

Figure 7. PGE_2 and FGF2 have opposite effects on myofibroblast proliferation and apoptosis. (**A**) CCL210 myofibroblasts were treated with PGE_2, FGF2, or PGE_2 + FGF2 for 24-72 h. qPCR analysis of the proliferation gene *FOXM1* was performed at 48 h while *CCNB2*, *CCND1*, and *CDKN1C* were assessed at 72 h (top panel). qPCR analysis of the anti-apoptotic gene *SERPINE1* was performed at 24 h while *BIRC5* and *MYC* were assessed at 48 h; the pro-apoptotic gene *CASP9* was assessed at 72 h. (**B**) Proliferation was assessed 96 h following treatment with PGE_2 and/or FGF2 by CyQUANT Cell Proliferation Assay. (**C**) Apoptosis sensitivity

was assessed by measuring total and cleaved CASP3 and PARP by Western blot analysis in myofibroblasts 5 d following addition of PGE_2 and/or FGF2 followed by treatment with the death receptor ligand anti-Fas. CASP3 was measured 30 min and PARP 1 h following anti-Fas treatment. Densitometry represents ratio of cleaved products to total protein. Relative fold changes of indicated genes measured by qPCR are normalized to *GAPDH*. Bars represent mean ± SEM. Data points represent replicate samples from three (**A** and **C**) or four (**B**) experiments. Lines indicate conditions being compared. Isolated asterisk indicates statistical significance compared with untreated myofibroblast. $*P < 0.05$, one-way ANNOVA. De-diff = De-differentiation.

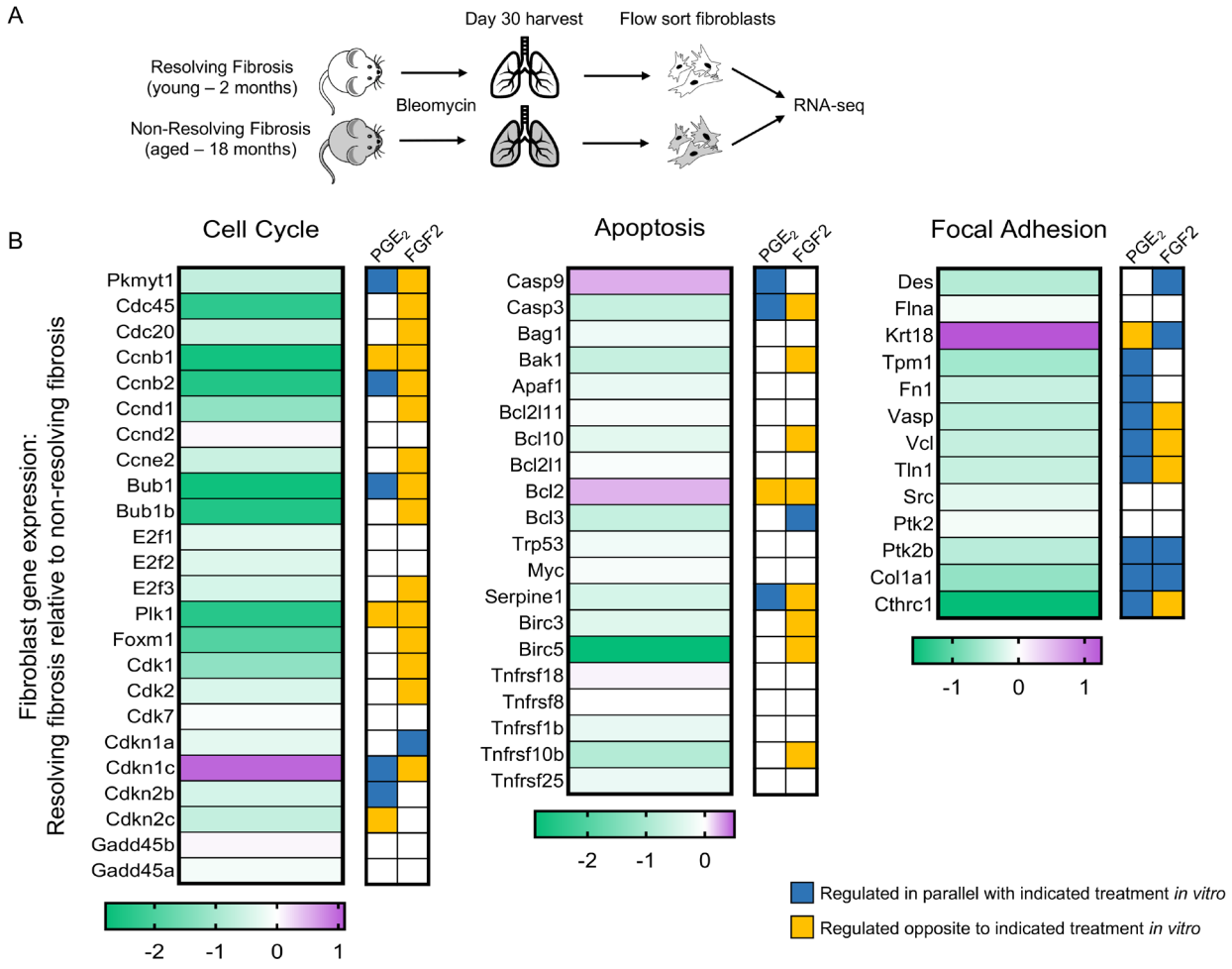

Figure 8. Lung fibroblasts from an in vivo model of fibrosis resolution exhibit similar gene signatures as those determined in myofibroblasts de-differentiated in vitro. (**A**) Experimental scheme for bleomycin-induced pulmonary fibrosis in Col1α1-GFP+ mice with resolving fibrosis (young) and non-resolving fibrosis (aged); mice were sacrificed on day 30 and fibroblasts were flow-sorted from

lungs and submitted for RNA-seq. (**B**) Heatmap display of gene expression in mice with resolving fibrosis (compared to the expression in mice with non-resolving fibrosis). Color scale depicts range of log2 fold changes in gene expression. *Tnfrsf10b* is the mouse homolog of human *TNFRSF10A*. Gene expression patterns regulated in parallel (blue) or opposite (yellow) to those exhibited with in vitro treatments of human myofibroblasts are indicated in color-filled boxes to the right of the heatmaps.

	KEGG Pathway	PGE_2		FGF2	
		DE genes (Total)	Adjusted p-value	DE genes (Total)	Adjusted p-value
Enriched by PGE_2 Only	MAPK signaling pathway	74 (263)	0.001	42 (251)	0.124
	cGMP-PKG signaling pathway	45 (140)	0.002	24 (131)	0.078
	Ras signaling pathway	59 (196)	0.006	28 (186)	0.436
	ErbB signaling pathway	20 (77)	0.008	11 (74)	0.323
	mTOR signaling pathway	33 (136)	0.013	12 (131)	1.000
	Apelin signaling pathway	36 (118)	0.018	17 (109)	0.194
Enriched by FGF2 Only	Cell cycle	27 (123)	0.523	31 (122)	0.001
	p53 signaling pathway	20 (69)	0.096	18 (67)	0.003
	Cell adhesion molecules	20 (107)	0.750	23 (92)	0.003
	ECM-receptor interaction	12 (78)	0.815	16 (75)	0.025
	JAK-STAT signaling pathway	34 (115)	0.085	23 (105)	0.032
	Gap junction	22 (79)	0.089	18 (71)	0.034
	Histidine metabolism	4 (17)	0.667	6 (16)	0.038
	Tryptophan metabolism	12 (37)	0.132	10 (31)	0.014
Enriched by both PGE_2 and FGF2	Cytokine-cytokine receptor interaction	61 (186)	1.07E-05	43 (154)	3.89E-05
	Hippo signaling pathway	54 (146)	1.59E-05	29 (136)	0.027
	cAMP signaling pathway	56 (172)	0.001	35 (154)	0.001
	Wnt signaling pathway	45 (141)	0.001	28 (130)	0.014
	TGF-beta signaling pathway	33 (87)	0.002	19 (85)	0.036
	PI3K-Akt signaling pathway	78 (297)	0.005	50 (279)	0.025
	Calcium signaling pathway	44 (153)	0.007	31 (133)	0.005
	TNF signaling pathway	33 (101)	0.032	24 (98)	0.007

Table 1: KEGG pathway enrichment following treatment with PGE_2 only, FGF2 only, or both PGE_2 and FGF2.

DE = differentially expressed genes.

lncRNA	Effect of PGE_2	Effect of FGF2	Effect on Fibrosis	miR interactions	Reference
PCAT1	↓↓↓	↓	Pro-fibrotic	sponges miR-145	(83, 84)
PVT1	↓↓	↑	Pro-fibrotic	sponges miR-214-3p	(85, 86)
NEAT1	↓	↓	Pro-fibrotic	sponges miR 27a	(42, 87)
DNM3OS	↓	↓	Pro-fibrotic	induces miR-214-3p, 199-3p/5p	(44)
MALAT1	↔	↓	Pro-fibrotic	sponges miR-199a-3p,125b	(43, 88, 89)
H19	↑↑	↔	Pro-fibrotic	sponges let-7 family	(86)
FENDRR	↑↑↑	↔	Anti-fibrotic	sponges miR-214	(45)
MEG3	↑	↔	Anti-fibrotic	sponges miR-21-5p, 29	(86, 90, 91)
GAS5	↓	↓	Anti-fibrotic	sponges miR-21	(92)

Table 2: Fibrotic effects and selected miRNA interactions of lncRNAs regulated by PGE_2 or FGF2. Arrows represent the following log2 fold changes: ↑ 0.5 to 1.0; ↑↑ 1.0 to 2.0; ↑↑↑ >2.0; ↓ -0.5 to -1.0; ↓↓ -1.0 to -2.0; ↓↓↓ < -2.0; ↔ NS.